Structural Engineering and Mechanics, *Vol. 64, No. 1 (2017) 59-69*
DOI: https://doi.org/10.12989/sem.2017.64.1.059

Fracture properties of concrete using damaged plasticity model -A parametric study

J.S. Kalyana Rama[*1], D.R. Chauhan[1a], M.V.N Sivakumar[2b], A. Vasan[1c] and A. Ramachandra Murthy[3d]

[1]*Department of Civil Engineering, BITS Pilani, Hyderabad Campus, Hyderabad, India*
[2]*Department of Civil Engineering, National Institute of Technology, Warangal, India*
[3]*CSIR-Structural Engineering Research Centre, Chennai, India*

(Received February 1, 2017, Revised June 28, 2017, Accepted July 10, 2017)

Abstract. The field of fracture mechanics has gained significance because of its ability to address the behaviour of cracks. Predicting the fracture properties of concrete based on experimental investigations is a challenge considering the quasi-brittle nature of concrete. So, there is a need for developing a standard numerical tool which predicts the fracture energy of concrete which is at par with experimental results. The present study is an attempt to evaluate the fracture energy and characteristic length for different grades of concrete using Concrete Damage Plasticity (CDP) model. Indian Standard and EUROCODE are used for the basic input parameters of concrete. Numerical evaluation is done using Finite Element Analysis Software ABAQUS/CAE. Hsu & Hsu and Saenz stress-strain models are adopted for the current study. Mesh sensitivity analysis is also carried to study the influence of type and size of elements on the overall accuracy of the solution. Different input parameters like dilatation angle, eccentricity are varied and their effect on fracture properties is addressed. The results indicated that the fracture properties of concrete for various grades can be accurately predicted without laboratory tests using CDP model.

Keywords: concrete damaged plasticity model; fracture mechanics of concrete; stress-strain relations; ABAQUS/CAE; numerical modelling

1. Introduction

Concrete is a strongly heterogeneous material and thus exhibits a complex nonlinear mechanical behaviour. Failure under tension and low confined compression are characterized by softening which is a phenomenon of decreasing stress with increasing deformations. This softening response is associated with a reduction of the unloading stiffness of concrete, and permanent deformations, which occur in thin zones called cracks. On the other hand, the behaviour of concrete under high confined compression is characterized by a ductile hardening response, which is, nothing but an increasing stress with increasing deformations. These phenomena should be considered in a constitutive model for analysing the multi-axial behaviour of any concrete structure.

Though there are many constitutive models for the nonlinear response of concrete proposed in the literature, commonly used frameworks are plasticity models, damage mechanics models, and combinations of plasticity and damage mechanics models. Stress-based plasticity models are useful for the modelling of concrete subjected to triaxle stress states since the yield surface corresponds to the strength envelope of concrete at a certain stage of hardening. Hence, a constitutive model based on the combination of damage mechanics and plasticity is to be developed to analyse the failure of concrete structures. The model should describe the important characteristics of the failure process of concrete subjected to multi-axial loading. This can be achieved by combining an effective stress based plasticity model with a damage model based on plastic and elastic strain measures. Then the model response in tension and under uniaxial, biaxial and triaxle compression can be compared with experimental results. The Concrete Damage Plasticity (CDP) model is an apt model and its modelling in the finite element software ABAQUS/CAE can help us understand the nonlinear response of concrete. However, to understand the CDP model, knowledge on some basic failure criteria and models is a prerequisite. Initial understanding of the failure criteria of concrete under varied loading conditions and alternate state of stresses is essential for assessing the behaviour of concrete. Later, inferences from certain experimental works and the features of the concrete failure have been discussed. This is followed by a study on prominent failure criteria such as the Tresca and Von-Mises etc. which are one parameter models and a comprehensive discussion on the Drucker-Prager failure model and its application to the CDP model was also studied. Failure theory is the phenomenon of predicting the

∗Corresponding author, M.Tech.
E-mail: kalyan@hyderabad.bits-pilani.ac.in
[a]B.E.
E-mail: f2013398@hyderabad.bits-pilani.ac.in
[b]Ph.D.
E-mail: mvns@nitw.in
[c]Ph.D.
E-mail: vasan@hyderabad.bits-pilani.ac.in
[d]Ph.D.
E-mail: murthyarc@serc.res.in

http://www.techno-press.com/journals/sem&subpage=7 ISSN: 1225-4568 (Print), 1598-6217 (Online)

conditions which cause failure of solid materials under the action of external loads. Two of the most significant concrete failure mechanisms are cracking under tension and crushing under compression. However, concrete strength observed under uniaxial compression or tension drastically varies from the one determined in complex states of stress. For example, the same concrete under biaxial compression reaches a strength of almost twenty percent higher than in the uniaxial state and under uniform triaxle compression, its strength is unlimited (theoretically). The behaviour of concrete changes radically when the nature of loading changes from compressive to tensile. Under uniaxial and biaxial tensile loads, the behaviour of concrete remains same. But, the same concrete exhibits different behaviour for uniaxial and biaxial compressive loads. Hence, the nature and type of loading play a vital role in the behaviour of concrete. In order to describe strength with the equation for triaxle stress, its plane should be presented in a three-dimensional stress space (since concrete is assumed to be an isotropic material in a wide range of stress). The states of stress on this surface correspond to material failure, whereas the states of safe behaviour are inside. Also, the so-called plastic potential surface is located inside this space. Once the plasticity surface is crossed, two cases may arise (Majewski 2003):

1. Ideal Plasticity condition (i.e., an increase in strain with no change in stress)
2. Rupture (material weakening)

To understand the actual behaviour of concrete in compression and tension, numerous analytical models have been developed. These models are formulated based on the microscopic and macroscopic behaviour of concrete. The models based on macroscopic behaviour are essentially used in practice especially in construction field (Kupfer and Gerstle 1973, Kotsovos and Newman 1977, Mills and Zimmerman 1970, Lee *et al.* 2004). The deformation patterns and stress-strain curves are the two vital indicators of the behaviour of concrete. In order to define completely the deformational and stress-strain behaviour of concrete, the structure must be analysed till failure. The deformation of the structure is linearly elastic till the yield limit, and beyond this point, plastic deformation (irreversible) occurs. A model chosen must be capable of exhibiting the above-mentioned behaviour till failure. One such way of obtaining a model is by utilizing the plasticity theory (Chen and Chen 1975). According to plasticity theory, yield limit is the limit below which the material property remains elastic and further loading beyond this point causes plastic flow. In the case of elastic-perfectly plastic, the initial yield surface becomes a failure/bounding surface, reflecting the increase in the strain without further change in stress. However, for concrete which has an elastoplastic behaviour, strain hardening and strain softening behaviour are to be included. Strain hardening is the region between the yield and peak stress which reflects the hardening nature of concrete with an increase in stress value. If the concrete hardens and attains the peak stress, further loading results in a decrease in stress with an increase in strain, hence enabling the softening behaviour. Thus, initial loading or yield surface is allowed to expand on the application of load resulting in the strain-hardening behaviour of concrete, defining the subsequent loading surface (Muthukumar and Kumar 2014).

2. Experimental behaviour of concrete

It is well known that the analysis of plain concrete is quite complex in terms of its failure and presence of reinforcement makes it more difficult. However, the conditions responsible for the local failure are almost the same for both of these and hence, an understanding of the failure criteria of plain concrete, too, is vital (Brestler and Pister 1958a, Brestler and Pister 1958b). Experimental results show that four parameters, namely uniaxial compressive strength, strain corresponding to uniaxial compressive strength, initial tangent modulus and ultimate strain at failure can be regarded as the characteristic values for the stress-strain curve of concrete under uniaxial compression (Brestler and Pister 1958a, Brestler and Pister 1958b). Also, the strength of concrete is dependent on the state of stress and it cannot be predicted without considering the interaction between stresses (Carreira and Chu 1985). The tensile strength of concrete was found to be almost equal under both uniaxial and biaxial stress conditions mentioned above but the biaxial compressive strength is higher than the uniaxial compressive strength and the compressive strength was found to decrease linearly with the increase in tensile stress under combined compression and tension (Kupfer *et al.* 1969, Kwak and Filippou 1990). Experiments also conclude that confinement of concrete significantly enhances the compressive strength of concrete (Gardner 1969, Chuan-Zhi *et al.* 1987). So, based on the above mentioned parameters, the Saenz Model, and Hsu and Hsu model had been developed to detail the compressive behaviour of concrete numerically.

2.1 Formulation of stress-strain curves in compression

The characteristic compressive strength, f_{ck}, is considered the base parameter. It is used to calculate mean compressive strength, f_{cm}, as per IS 456:2000 (Cement and Concrete Sectional Committee, CED 2 2000), as follows

$$f_{cm} = f_{ck} + 1.65\sigma \tag{2.1}$$

where, σ, the standard deviation, is given as

$$\begin{aligned} \sigma &= 3.5 \text{ MPa; if } f_{ck} = 10{,}15 \text{ MPa} \\ \sigma &= 4.0 \text{ MPa; if } f_{ck} = 20{,}25 \text{ MPa} \\ \sigma &= 5.0 \text{ MPa ; if } f_{ck} \geq 30 \text{ MPa} \end{aligned} \tag{2.2}$$

The moduli of elasticity as per European (European Committee for Standards 2008), and Indian standard codes of practice are given as

$$\begin{aligned} E_{cm} &= 22000(0.1 \cdot f_{cm})^{0.3}; \text{ EUROCODE 2} \\ E_{cm} &= 5000\sqrt{f_{ck}} \text{ ; IS 456:2000} \end{aligned} \tag{2.3}$$

where, E_{cm}, f_{cm}, and f_{ck} are in MPa.

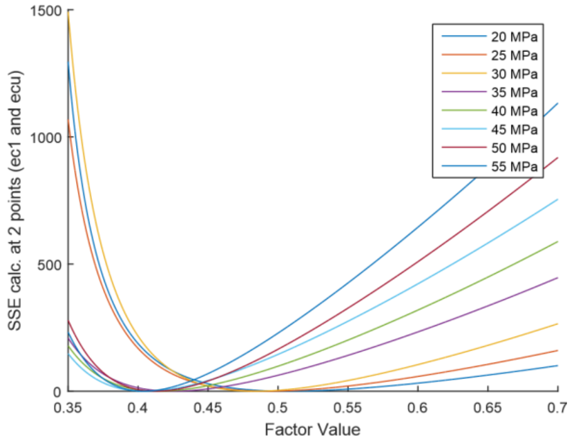

Fig. 1 Sum-Squared-Errors vs. Factor Value (for IS 456:2000)

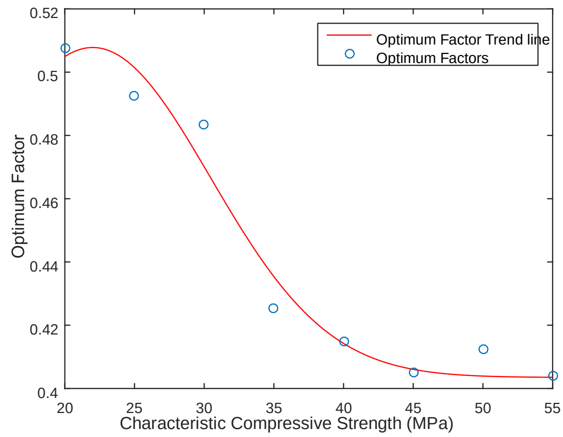

Fig. 2 *Correction Factor* vs. Characteristic Compressive Strength (for IS 456:2000)

Table 1 Correction factor values

Characteristic Compressive Strength (MPa)	Correction Factor IS 456:2000	Correction Factor EURO-CODE 2
20	0.5077	0.5764
25	0.4926	0.5468
30	0.4836	0.5294
35	0.4252	0.4605
40	0.4148	0.4416
45	0.4052	0.4246
50	0.4124	0.4256
55	0.4040	0.4115

2.1.1 Saenz formula

Saenz Formulation (Saenz 1964) consists of a Rational Function whose denominator is 3rd degree polynomial and numerator is 1st degree polynomial. The refined formulation of Saenz model by Kmiecik and Kamiński (2011), is given as follows

$$\sigma_c = \frac{\varepsilon_c}{A + B\varepsilon_c + C\varepsilon_c^2 + D\varepsilon_c^3} \tag{2.4}$$

where, the parameters are given as

$$\begin{gathered} A = \frac{1}{E_{cm}}; B = \frac{P_3 + P_4 - 2}{P_3 f_{cm}} \\ C = -\frac{2P_4 - 1}{P_3 f_{cm}\varepsilon_{c1}};\ D = \frac{P_4 - 1}{P_3 f_{cm}\varepsilon_{c1}} \\ P_1 = \frac{\varepsilon_{cu}}{\varepsilon_{c1}};\ P_2 = \frac{f_{cm}}{f_{cu}} \\ P_3 = \frac{E_{cm}\varepsilon_{c1}}{f_{cm}}; P_4 = \frac{P_3(P_2 - 1)}{(P_1 - 1)^2} - \frac{1}{P_2} \end{gathered} \tag{2.5}$$

The parameters ε_{c1} and ε_{cu} are defined as strain at maximum compressive stress and ultimate compressive strain, respectively. Accurate quantification of these parameters was given by Majewski (2003), as follows

$$\begin{aligned} \varepsilon_{c1} &= 0.0014[2 - \exp(-0.024 f_{cm}) \\ &\quad - \exp(-0.140 f_{cm})] \\ \varepsilon_{cu} &= 0.004 - 0.0011[1 - \exp(-0.0215 f_{cm})] \end{aligned} \tag{2.6}$$

These four parameters, viz. f_{cm}, ε_{c1}, f_{cu} and ε_{cu}, need to be known to obtain the Saenz Curve. Generally, f_{cu} is unknown, and some value needs to be assumed to generate Saenz curve.

Factor Value is defined as the ratio of f_{cu} to f_{cm}. It is found that, for any random *Factor Value*, the generated Saenz curve does not pass through

(ε_{c1}, fcm) and (ε_{cu}, f_{cu}). The *Factor Value* for which the Saenz curve passes through the above-mentioned reference points is termed as *Correction Factor*. It is obtained by minimizing least-squared-errors of stress values at abscissae of ε_{c1} and ε_{cu}. Fig. 1 depicts the optimization scheme. Fig. 3 shows the generated Saenz Curve passes through the reference points, which happens if *Factor Value*= *Correction Factor*. Fig. 4 shows that the generated Saenz Curve does not pass through the reference points as the *Factor Value* ≠ *Correction Factor*. Hence, it is required to incorporate *Correction Factor* in existing Saenz Model.

The *Correction Factor* values obtained using E_{cm} value as per IS 456:2000 and EUROCODE 2 are shown in Table 1. The *Factor Value*, from Fig. 1, at minimum Sum-Squared-Errors is the *Correction Factor*. The obtained *Correction Factor*s are regressed against f_{ck} to obtain a trend line. The equation, using IS 456:2000, for which is

$$\begin{gathered} CorrectionFactor \\ = 0.1043 \cdot exp\left(-\left(\frac{f_{ck} - 22}{11.94}\right)^2\right) + 0.4035 \end{gathered} \tag{2.7}$$

and, using EUROCODE 2 is

$$\begin{gathered} CorrectionFactor = \\ 0.1887 \cdot exp\left(-\left(\frac{f_{ck} - 14.75}{21.27}\right)^2\right) + 0.4 \end{gathered} \tag{2.8}$$

The goodness parameters of the fit (Eqs. (2.7) and (2.8)) are: R^2=0.9965 and 0.9731, *RMSE*=0.0080 and 0.0105, and *SSE*=4.45×10^{-4} and 7.7183×10^{-4} for IS 456:2000 and EUROCODE 2 respectively. The fit can be visualised in Fig. 2. By substituting the value of *Correction Factor* in Saenz Equation, we can model the compressive stress-strain curve. A typical stress-strain curve generated by Saenz Model is shown in Fig. 3. The reference points are (f_{cm}, ε_{c1}) and (f_{cu}, ε_{cu}) where, $f_{cu} = f_{cm}$ × *Factor Value*. Factor Value can

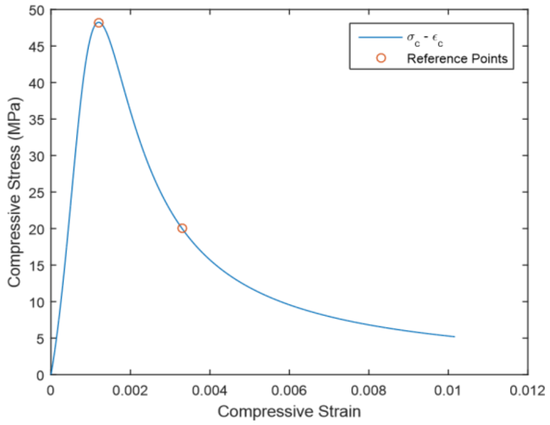

Fig. 3 Saenz Curve for M40 gradeconcrete
(Factor Value=Correction Factor)

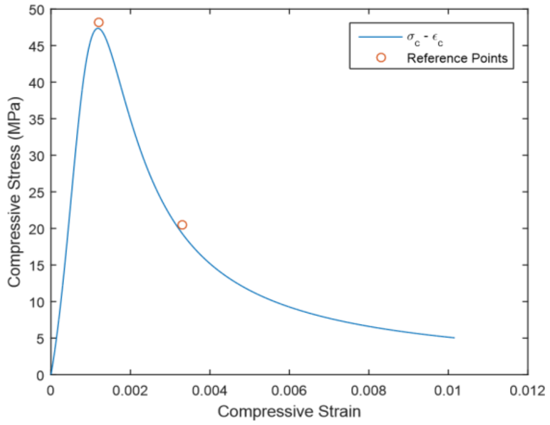

Fig. 4 Saenz Curve for M40 grade concrete
(*Factor Value=Correction Factor*)

be any ratio of f_{cu} to f_{cm}. If, Factor Value=Correction Factor, the plot will pass through both the points, otherwise it will not. An example of such case is shown in Fig. 4, where the Correction Factor is 0.4148 (*M*40), but we adopt Factor Value as 0.4252 (≈2.5% deviation) while modelling. We can observe that the plot fails to pass to through the reference points.

2.1.2 Hsu & Hsu formula

The numerical model proposed by Hsu and Hsu (1994) has the capacity to develop compressive stress-strain relation till $0.3\sigma_{cu}$ in the descending portion of the stress-strain curve. This model is appropriate for both normal, and high strength concretes with minor modifications. The input parameters required for the model are σ_{cu} (also, f_{cm}) and E_{cm}. No modifications are necessary for normal concretes up to 62 MPa (≈M55 grade). Modifications for high strength concretes are detailed in Hsu and Hsu (1994).

The model for normal strength concrete is described below

$$\sigma_c = E_{cm} \cdot \varepsilon_c \qquad ; \text{if } \sigma_c \leq 0.5\sigma_{cu}$$

$$\sigma_c = \left(\frac{\beta \cdot {}^{\varepsilon_c}/_{\varepsilon_o}}{\beta - 1 + \left({}^{\varepsilon_c}/_{\varepsilon_o} \right)^{\beta}} \right) \sigma_{cu} \qquad ; \text{till } \sigma_c = 0.3\sigma_{cu} \tag{2.9}$$

The parameter ε_o is the strain at maximum stress (σ_{cu}) and the parameter β, which depends on the shape of the stress-strain curve, are given as

$$\varepsilon_o = 8.9 \times 10^{-5}\sigma_{cu} + 2.114 \times 10^{-3} \tag{2.10}$$

$$\beta = \frac{1}{1 - \frac{\sigma_{cu}}{\varepsilon_o E_{cm}}} \tag{2.11}$$

Note: For the above equations, the parameters σ_c, σ_{cu}, and E_{cm} are in $^{\text{kip}}/\text{in}^2$. (1MPa = 0.145037743 $^{\text{kip}}/\text{in}^2$).

The inelastic compressive strain (ε_c^{1n}) is defined as the difference between total compressive strain (ε_c) and elastic compressive strain (ε_c^{el}).

ABAQUS/CAE requires the damage variation with respect to inelastic strain. As quantification of damage propagation is difficult, many theories have been put forth to quantify it (Birtel and Mark 2006, López-Almansa *et al.* 2014). Here, the compressive damage (d_c) is calculated as the ratio of inelastic strain at the point to the total strain (Wahalathantri 2012).

2.2 Formulation of stress-strain curves in tension

Here, for all simulated cases, only 2 values, one at maximum tensile stress and another at zero tensile stress, are adopted while modelling.

Tensile Stress	Cracking Strain	Tensile Damage
X	0	0
0	0.01	0.9

3. Determination of size independent fracture energy and characteristic length

3.1 Fracture energy

3.1.1 Boundary Effect Method (BEM)

It is found that the local fracture energy varies with the width of the fracture process zone (FPZ). The FPZ becomes more and more restricted as it reaches the stress-free back of the specimen. As a result, the local specific fracture energy reduces as the crack reaches the back end. Hu and Wittmann (1992) were the first to observe this phenomenon. They observed that initially when the crack starts to grow from a pre-existing notch, the rate of decrease is negligible, but it accelerates as it reaches the stress-free back. They modelled this behaviour bilinear, after performing extensive tests.

They also came up with the relationship

$$G_f(a, D) = \frac{\int_0^{D-a} g_f(x)dx}{D - a}$$
$$= \begin{cases} G_F\left[1 - \dfrac{{}^{a_l}/_D}{2\left(1 - {}^{a}/_D\right)}\right]; 1 - {}^{a}/_D > {}^{a_l}/_D \\ G_F \cdot \dfrac{\left(1 - {}^{a}/_D\right)}{2 \cdot {}^{a_l}/_D} \qquad ; 1 - {}^{a}/_D \leq {}^{a_l}/_D \end{cases} \tag{3.1}$$

Where,

G_f represents size dependent fracture energy calculated

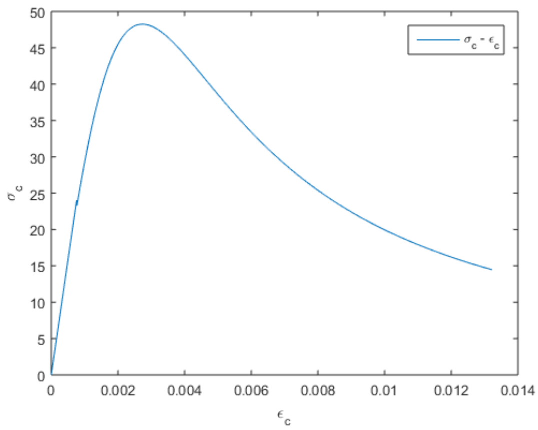

Fig. 5 Stress-Strain curve generated by Hsu & Hsu model for M40 grade of concrete

by RILEM work-of-fracture method.

G_F represents size independent specific fracture energy.

a_l represents transition ligament length.

a/D represents initial crack to depth ratio.

After testing a lot of specimens, an over-determined set of equations is obtained, to determine G_F and a_l which is solved by using the method of least squares.

Karihaloo *et al.* (2003) found out that this lengthy procedure need not be applied. It was proposed to take specimens of the same size and separate the crack-to-depth ratio by large amount say, 0.05 & 0.5 or 0.1 & 0.6, with a restriction on aggregate size depending on span-to-depth ratio, which will provide an exact solution which is very close to the solution proposed by Hu and Wittmann.

According to theory, at the start of load application on the notched specimen, the size of FPZ increases, then remains approximately constant for a certain range and then decreases as the crack reaches the stress-free back boundary of the specimen. This procedure gives better accuracy but is a time-consuming process requiring acoustic emission setup. Hence, the bilinear approximation is generally adopted.

3.1.2 P − δ tail correction method

Guinea *et al.* (1992), Planas *et al.* (1992), and Elices *et al.* (1992) identified several sources of energy dissipation that influence the measurement of G_f by the RILEM work-of-fracture method RILEM Technical Committee 50-FMC (1985). They found most of them were due to experimental errors. The major part of the same was found to be the unrecorded energy at the tail of the *P*−*δ* curve which failed to reach *P*=0. They modelled the remaining part of the *P*−*δ* curve, i.e., Beam behaviour at low loads when the crack reached the free surface, as linear.

The relationship they developed was

$$G_F = \frac{\left(\int_0^{\delta_u} P d\delta\right) + W_{nm}}{b(D-a)} \tag{3.2}$$

Where *b* (*D*−*a*) represents the area of the ligament at the start of the test.

3.2 Characteristic length

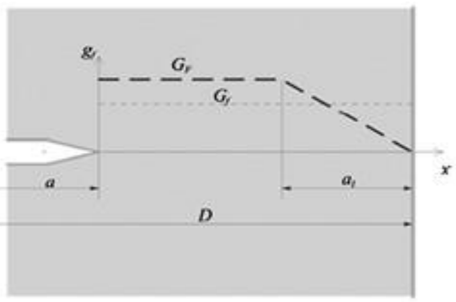

Fig. 6 Bilinear tension softening (Murthy *et al.* 2013)

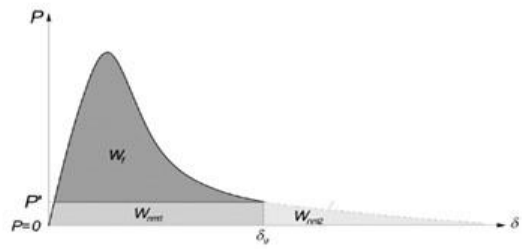

Fig. 7 *P*−*δ* tail correction Murthy *et al.* (2013)

Hillerborg *et al.* (1976) proposed the Fictitious crack model in 1976, which assumes that the crack propagation occurs when principal tensile stress reached the tensile strength of the material (f_t) and that the energy required to create new surfaces is negligible when compared to that required to separate them. The model introduces a material parameter, namely, characteristic length (l_{ch}), which depends on three other material parameter: size-independent fracture energy (G_F), the tensile strength of the material (f_t) and modulus of elasticity (*E*).

$$l_{ch} = \frac{E \cdot G_F}{f_t^2} \tag{3.3}$$

This parameter is proportional to the length of the fracture process zone.

4. Results and discussion

ABAQUS/CAE software package is used for analysing the behaviour of beam under TPB test.

The beam of size 500 mm×100 mm×100 mm is adopted for the present study. The notch width is adopted as 2 mm for all the simulated cases. Plasticity of concrete is modelled using Concrete Damaged Plasticity module available in ABAQUS/CAE. The sample meshing for *a/D*=0.1 and 0.6 are shown in Fig. 8. The load-displacement curves are generated as output. Using these load-displacement curves, fracture energy (G_f) for each simulation is obtained using RILEM work-of-fracture method. The size-independent fracture energy (G_F) is obtained using the modified boundary effect model (Murthy *et al.* 2013, Karihaloo *et al.* 2003). The characteristic length is obtained from expression proposed by Hillerborg *et al.* (1976).

The study of the effect on the variation of mesh element type, mesh element size, grade of concrete, the model used

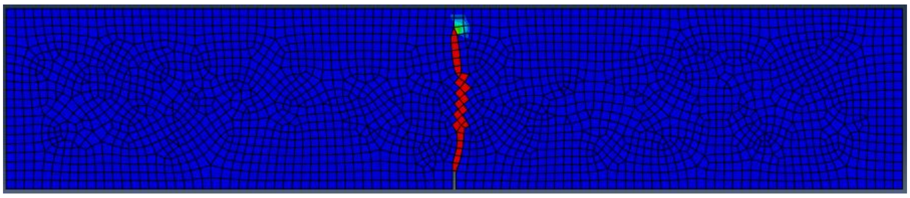

(a) *a/D*=0.1

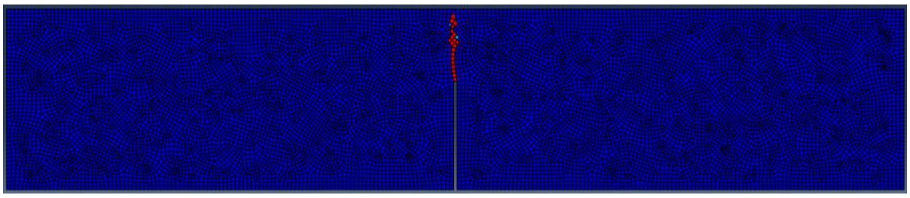

(b) *a/D*=0.6

Fig. 8 Tensile damage propagation path

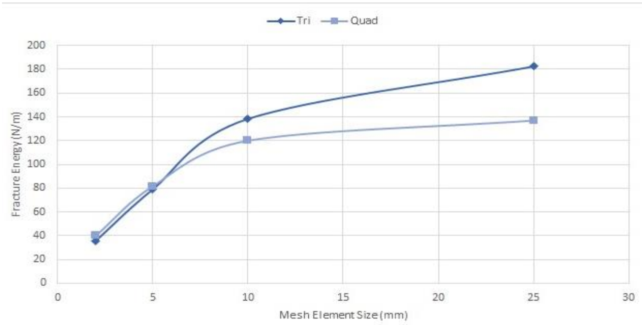

Fig. 9 Effect on fracture energy with variation in mesh element type and size

for calculation of compressive behaviour, final tensile damage value, dilation angle, eccentricity, and notch-to-depth ratio on fracture parameters is done. The results of the same are summarized further in this section.

4.1 Mesh element: type and size

The mesh element type is varied among quadrilateral or triangular elements. The mesh element sizes adopted for mesh dependency are 2 mm, 5 mm, 10 mm, and 25 mm. This study is done by modelling beam with *a/D*=0.1. The CDP data is adopted from Upreti *et al*. (2016).

From Fig. 9, the difference between fracture energies of 25 mm and 2 mm mesh element sizes are 146.7 N/m and 97.0 N/m for triangular and quadrilateral meshing, respectively. For 2 mm and 5 mm mesh element sizes the fracture energies for quadrilateral and triangular elements are almost equal.

4.2 Notch-to-depth ratio (a/D)

The variation in the notch-to-depth ratio is done from 0.1 to 0.6 with intervals of 0.1. This study is done for M50 grade of concrete with Eccentricity (ϵ) 0.01, Dilation Angle (ψ) 34°, Young's Modulus (E_{cm}) value as per IS 456:2000, and compression behaviour modelled as per Hsu and Hsu model.

The mesh size is varied for each *a/D* such that each uncracked ligament length (*D*−*a*) is divided into 18 equal

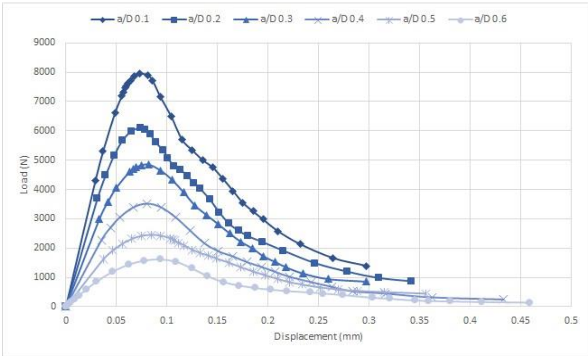

Fig. 10 Load-Displacement curves for different notch-to-depth ratios (M50 Grade Concrete)

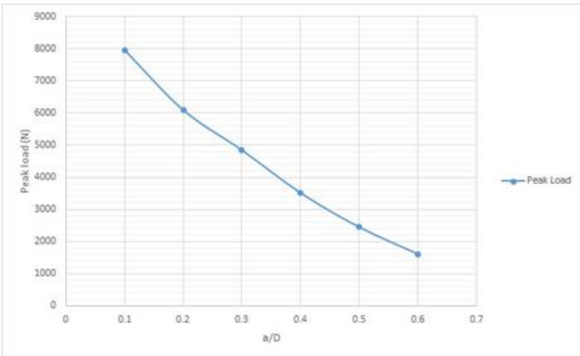

Fig. 11 Effect on peak loads with varying notch-to-depth ratios (M50 Grade Concrete)

parts.

From Figs. 10 and 11, the peak loads for each notch-to-depth ratio from 0.1 to 0.6, in same order, are: 7961 N, 6094 N, 4846N, 3518 N, 2455 N, and 1615 N. The residual loads for each notch-to-depth ratios, from 0.1 to 0.6, are: 1397 N, 873 N, 856 N, 248 N, 450 N, and 141 N respectively. The average ratio of residual load to peak load is 13.9%, with a standard deviation of 2.2%. From Fig. 12, the fracture energies at each notch-to-depth ratio from 0.1 to 0.6, in order, are: 133.3 N/m, 120.3 N/m, 105.5 N/m, 96.5 N, 86.8 N/m, and 71.8 N/m, respectively. These values follow a linear trend with R^2 value of 0.994 and *RMSE* value of 1.59 N/m.

Table 2 Summary of FE modelling for various mesh element types and sizes

Mesh element type	Mesh element size	no. of elements	no. of nodes
Quadrilateral	2	15286	15362
	5	2417	2501
	10	596	651
	25	108	133
Triangular	2	25761	13187
	5	4259	2253
	10	1091	608
	25	205	129

Table 3 Summary of FE modelling for various notch-to-depth ratios

Notch-to-depth ratio	Mesh element size	no. of elements	no. of nodes
0.1	5	2417	2501
0.2	4.44	3036	3158
0.3	3.89	3996	4097
0.4	3.33	5396	5522
0.5	2.78	7764	7893
0.6	2.22	12356	12478

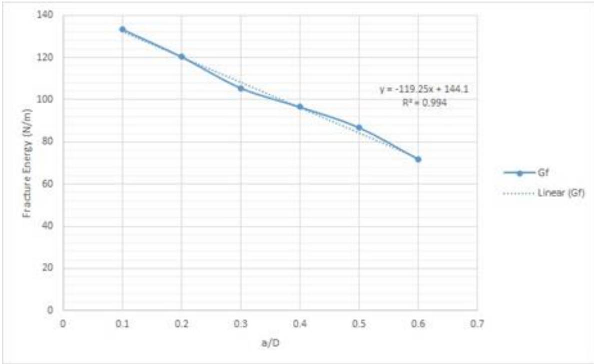

Fig. 12 Effect on fracture energy with variation in notch-to-depth ratio (M50 Grade Concrete)

4.3 Eccentricity (ϵ) and Dilation Angle (ψ)

The CDP parameters, Eccentricity (ϵ) and Dilation Angle (ψ), are varied to investigate their effect on fracture energy and characteristic length. The beams are modelled for E_{cm} values as per IS 456:2000 and compressive behaviour as per Hsu and Hsu model. This study has been done for M20 and M40 grades of concrete. From Fig. 13,

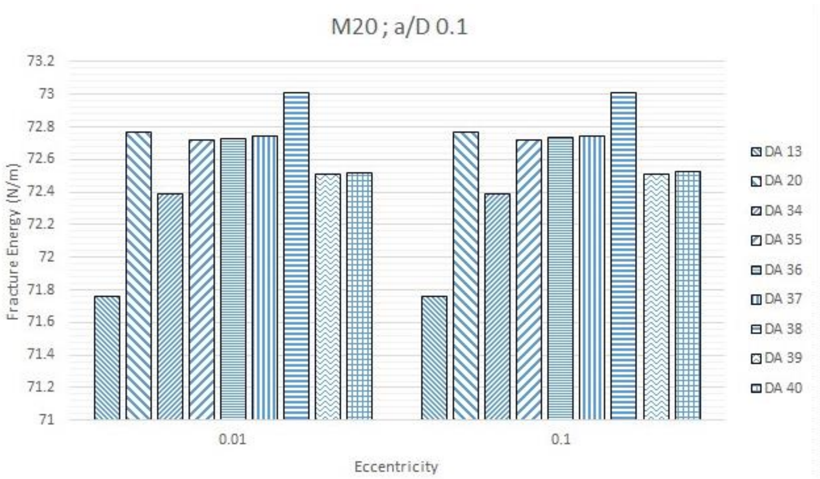

(a) M20 grade of concrete

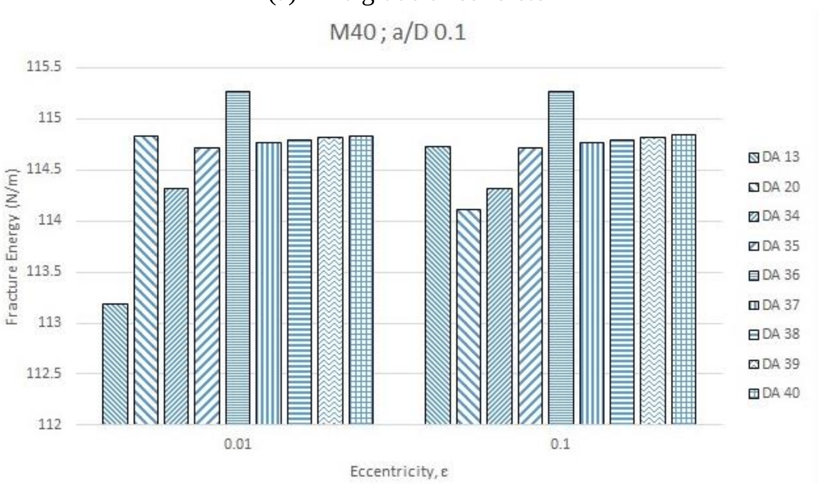

(b) M40 grade of concrete

Fig. 13 Effect on Fracture energy with variation in ϵ and ψ (*a/D*=0.1)

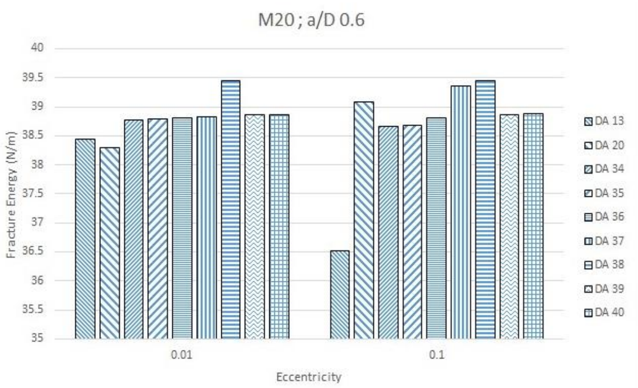

(a) M20 grade of concrete

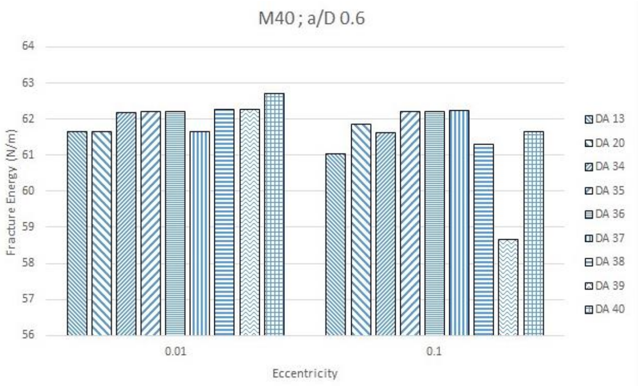

(b) M40 grade of concrete

Fig. 14 Effect on Fracture energy with variation in ϵ and ψ (a/D=0.6)

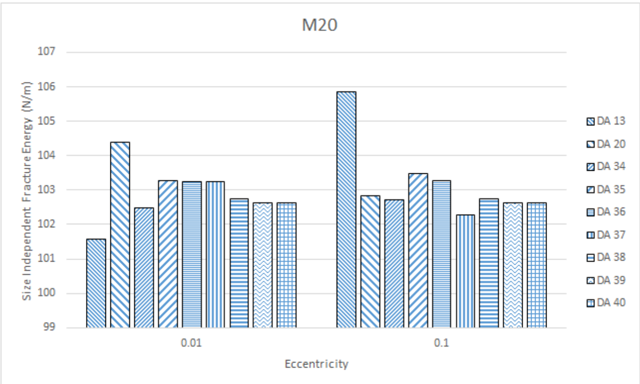

(a) M20 grade of concrete

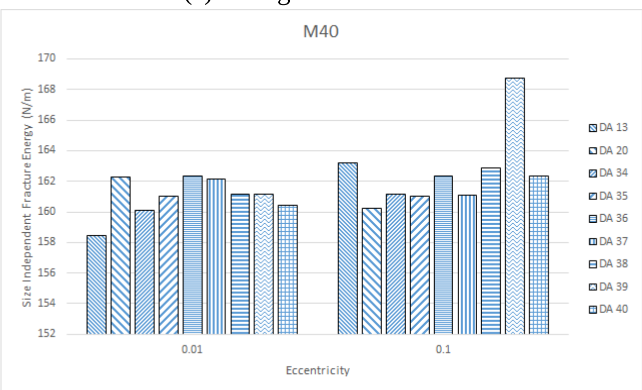

(b) M40 grade of concrete

Fig. 15 Effect on Size Independent Fracture energy with variation in ϵ and ψ

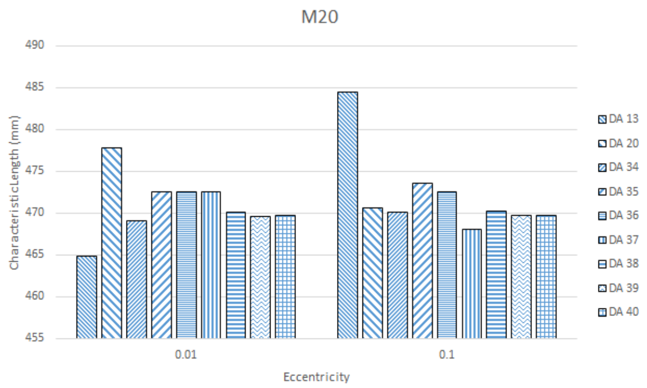

(a) M20 grade of concrete

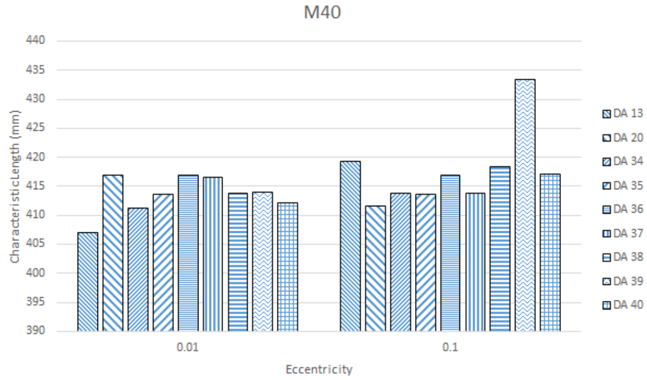

(b) M40 grade of concrete

Fig. 16 Effect on Size Independent Fracture energy with variation in ϵ and ψ

the average fracture energy for M20 and M40 grade of concrete with notch-to-depth ratio 0.1 are 72.6 N/m and 114.6 N/m for eccentricity 0.01, and 72.6 N/m and 114.7 N/m for eccentricity 0.1, respectively. The maximum percentage deviations from the average values, in same order as above, are 1.12%, 1.24%, 1.12% and 0.52%. Similarly, from Fig. 1, the average fracture energy for M20 and M40 grade of concrete with notch-to-depth ratio 0.6 are 38.8 N/m and 62.1 N/m for eccentricity 0.01, and 38.7 N/m and 61.4 N/m for eccentricity 0.1, respectively. The maximum percentage deviations from the average values, in same order as above, are 1.70%, 0.99%, 5.64% and 4.48%.

From Fig. 15, the average size-independent fracture energy for M20 and M40 grade of concrete are 102.9 N/m and 161.0 N/m for eccentricity 0.01, and 103.2 N/m and 162.6 N/m for eccentricity 0.1, respectively. The maximum % deviations from the average values, in same order as above, are 1.44%, 1.60%, 2.62% and 3.80%. From figure (16), the average characteristic length for M20 and M40 grade of concrete are 471.0 mm and 413.6 mm for eccentricity 0.01, and 472.1 mm and 417.5 mm for eccentricity 0.1, respectively. The maximum percentage deviations from the average values, in same order as above, are 1.44%, 1.60%, 2.62% and 3.80%.

4.4 Grade of concrete and model used for determination of compressive behaviour

As discussed in section (2.1), compression behaviour is

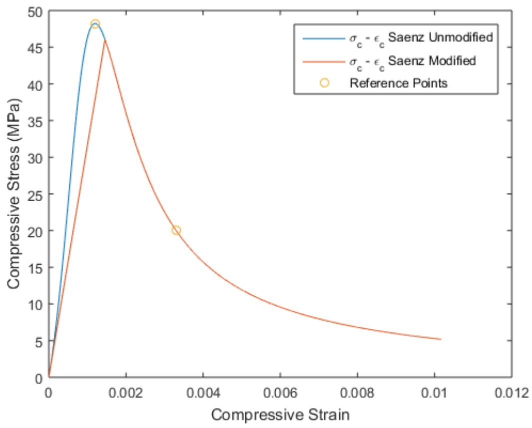

Fig. 17 Saenz Model Compression Curve (M40) - with and without modification

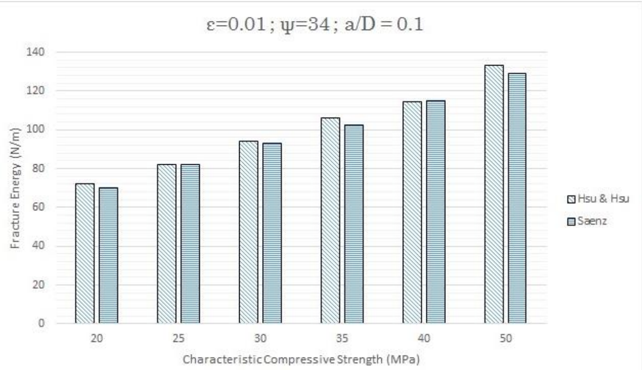

Fig. 18 Effect on fracture energy with varying grade of concrete and compressive behaviour design model (*a/D*=0.1)

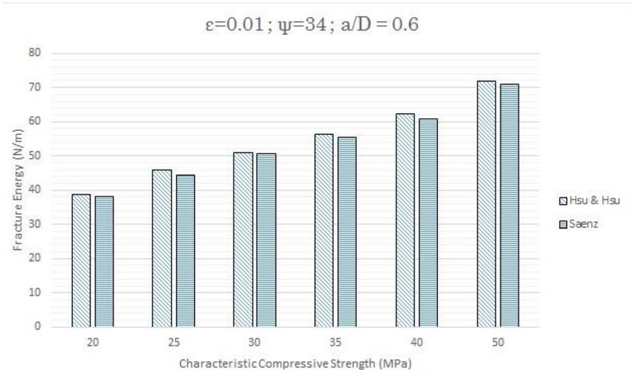

Fig. 19 Effect on fracture energy with varying grade of concrete and compressive behaviour design model (*a/D*=0.6)

modelled in two different ways. It was found that the initial tangent modulus while modelling compressive stress-strain curve using Saenz model was more than the input value of E_{cm}. Thus, one more refinement is proposed and carried out for Saenz Model. The initial part of the Saenz model is substituted with a straight line passing through the origin and slope E_{cm} until the line intersects the Saenz Curve as explained in section 2.1.1. The Fig. 17 shows the described modification. This modification leads to a decrease in the

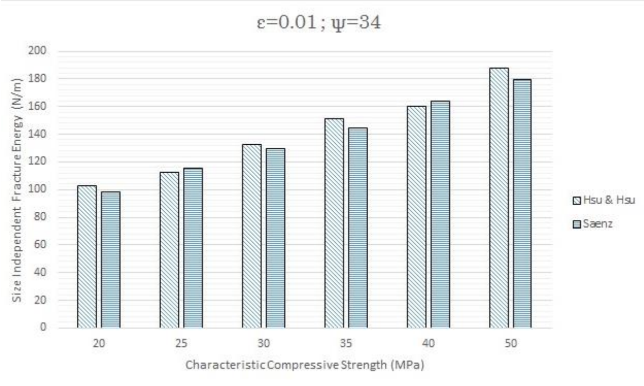

Fig. 20 Effect on Size-independent fracture energy with varying grade of concrete and compressive behavior design model

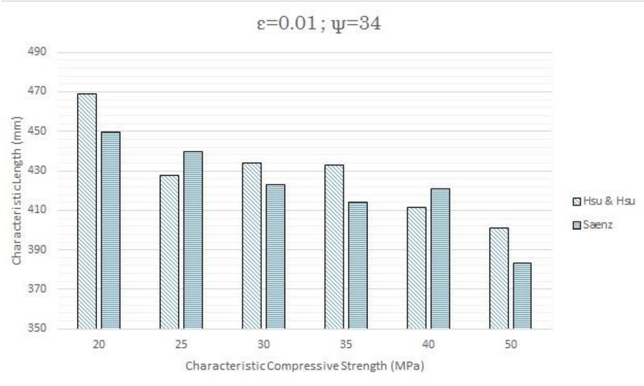

Fig. 21 Effect on characteristic length with varying grade of concrete and compressive behaviour design model

peak stress for grades of concrete above M25 but it is necessary to refrain it from generating negative inelastic and plastic strain values.

The value of eccentricity for this study is adopted to be 0.01, Dilation angle is 34°, and E_{cm} values is adopted as per IS 456:2000. The effect of adopting different model on fracture energy and characteristic length is discussed below.

From Fig. 18, the fracture energy for notch-to-depth ratio 0.1 increases at an average of 10.5 N/m (standard deviation=1.1 N/m) for each subsequent grade of concrete starting from M20 to M40 for Hsu & Hsu Model. The average for Saenz Model is 11.1 N/m (standard deviation = 0.7 N/m). The fracture energy values, for notch-to-depth ratio

0.1, obtained using Saenz model are, at an average, 1.8 N/m (standard deviation=0.9 N/m) less than those obtained using Hsu & Hsu model. From Fig. 19, the fracture energy for notch-to-depth ratio 0.6 increases at an average of 5.9 N/m (standard deviation=0.5 N/m) for each subsequent grade of concrete starting from M20 to M40 for Hsu & Hsu Model. The average for Saenz Model is 5.6 N/m (standard deviation=0.4 N/m). The fracture energy values, for notch-to-depth ratio 0.6, obtained using Saenz model are, at an average, 0.9 N/m (standard deviation=0.2 N/m) less than those obtained using Hsu & Hsu model. From Fig. 20, the size independent fracture energy increases at an average of 14.4 N/m (standard deviation=3.2 N/m) for each subsequent

Table 4 Validation of numerical work-2

Notch-to-depth Ratio	Fracture Energy (N/m) Value Numerical Model M50 (f_{cm} = 58.18 MPa)	Murthy *et al.* (2013) NSC (f_{cm} = 57.1 MPa)
0.1	133.3	135.3
0.2	120.3	107.5
0.3	105.5	95.5
	as per Modified BEM	as per BEM
Size-Independent	188.1	190.3

Table 5 Validation of numerical work-2

Notch-to-depth Ratio	Fracture Energy Value ($^N/m$) Numerical Model Hsu and Hsu M30	Saenz M30	Alyhya *et al.* (2016) Mix 30A
	(f_{cm}=38.20 MPa)	(f_{cm}=37.49 MPa)	(f_{cm}=35.4 MPa)
0.1	94.3	92.8	96.2
0.6	50.9	50.7	53.5
	as per Modified BEM		
Size-Independent	132.9	129.7	132.8

grade of concrete starting from M20 to M40 for Hsu & Hsu Model. The average for Saenz Model is 16.4 N/m (standard deviation=1.5 N/m). The size-independent fracture energy values, obtained using Saenz model are, at an average, 2.6 N/m (standard deviation=2.2 N/m) less than those obtained using Hsu & Hsu model. From Fig. 21, the characteristic length decreases at an average of 14.4 mm (standard deviation=12.4 mm) for each subsequent grade of concrete starting from M20 to M40 for Hsu & Hsu Model.

The average for Saenz Model is 7.2 mm (standard deviation=5.7 mm). The characteristic length values obtained using Saenz model are, at an average, 7.6 mm (standard deviation=6.6 mm) less than those obtained using Hsu & Hsu model.

5. Experimental validation

From Table 4, the percentage difference of the numerical values from the experimental values (Murthy *et al.* 2013) for notch-to-depth ratios 0.1, 0.2, and 0.3 are 1.48%, −11.91%, and −10.47% respectively. The percentage difference in the numerically obtained size-independent fracture energy (using modified BEM) and the experimentally obtained size-independent fracture energy is 1.16%

From Table 5, the percentage difference of the numerical fracture energy values from the experimental fracture energy values (Alyhya *et al.* 2016) for notch-to-depth ratios 0.1 are 1.98% and, 3.53% for Hsu & Hsu model, and Modified Saenz Model, respectively. The percentage difference values for notch-to-depth ratio 0.6 are 4.86% and 5.23%, for Hsu & Hsu model, and Modified Saenz Model respectively. The percentage differences in the numerically obtained size-independent fracture energies (using modified BEM) and the experimentally obtained size-independent fracture energy are −0.08% and 2.33%, for Hsu & Hsu, and Saenz model respectively.

6. Conclusions

- The Saenz Model is successfully modified to the needs of Concrete Damaged Plasticity model, such that it doesn’t generate negative inelastic strain values.
- Due to high deviations in peak loads in triangular elements with an increase in mesh size, quadrilateral elements should be preferred.
- A reduction in peak loads and fracture energy is observed while increasing the notch-to-depth ratio. The strain-softening behaviour is negligibly affected with increase in the notch-to-depth ratio.
- The change in the eccentricity and the dilation angle has negligible impact on both, fracture energy and characteristic length.
- Fracture energy increases and characteristic length decreases with an increase in the characteristic compressive strength of concrete, using both, Hsu & Hsu, and Saenz models.
- The proposed CDP model is able to predict fracture properties of concrete which are at par with the experimentally obtained values.

References

Alyhya, W., Dhaheer, M.A., Al-Rubaye, M. and Karihaloo, B. (2016), “Influence of mix composition and strength on the fracture properties of self-compacting concrete”, *Constr. Build. Mater.*, **110**, 312-322.

Birtel, V. and Mark, P. (2006), “Parameterised finite element modelling of RC beam shear failure”, *2006 ABAQUS Users Conference*.

Brestler, B. and Pister, K.S. (1958a), “Behaviour of concrete under triaxle compressive-compressive-tensile stresses”, *ACI Mater. J.*, **8**(2), 181-185.

Brestler, B. and Pister, K.S. (1958b), “Strength of concrete under combined stresses”, *Proc. ACI J.*, **55**, 321-345.

Carreira, D.J. and Chu, K.H. (1985), “Stress-strain relationship for plain concrete in compression”, *Proc. ACI J.*, **82**, 797-804.

Cement and Concrete Sectional Committee, CED 2 (2000), Indian Standard Plain and reinforced concrete-code of practice (IS 456: 2000), Bureau of Indian Standards.

Chen, A.C. and Chen, W.F. (1975), “Constitutive relations for concrete”, *J. Eng. Mech.*, **101**(4), 465-481.

Chuan-Zhi, W., Zhen-Hai, G. and Xiu-Qin, Z. (1987), “Experimental investigation of biaxial and triaxle compressive concrete strength”, *ACI Mater. J.*, **84**(2), 92-100.

Elices, M., Guinea, G. and Planas, J. (1992), “Measurement of the fracture energy using three-point bend tests: Part 3-influence of cutting the P- tail”, *Mater. Struct.*, **25**(6), 327-334.

European Committee for Standards, E.C. (2008), BS EN 1992-1-1 - Design of concrete structures. General rules and rules for buildings, CEN, Brussels.

Gardner, N.J. (1969), “Triaxial behaviour of concrete”, *Proc. ACI J.*, **66**, 136-158.

Guinea, G., Planas, J. and Elices, M. (1992), “Measurement of the fracture energy using three-point bend tests: Part 1-Influence of experimental procedures”, *Mater. Struct.*, **25**(4), 212-218.

Hillerborg, A., Moder, M. and Petersson, P.E. (1976), “Analysis of crack formation and crack growth in concrete by means of fracture mechanics and finite elements”, *Cement Concrete Res.*, **6**(6), 773-782.

Hsu, L.S. and Hsu, C.T. (1994), “Stress-strain behaviour of steelfiber high-strength concrete under compression", *ACI Struct. J.*, **91**(4), 448-457.

Hu, X.Z. and Wittmann, F. (1992), "Fracture energy and fracture process zone", *Mater. Struct.*, **25**(6), 319-326.

Karihaloo, B., Abdalla, H. and Imjai, T. (2003), "A simple method for determining the true specific fracture energy of concrete", *Mag. Concrete Res.*, **55**(5), 471-481.

Kmiecik, P. and Kamin´ski, M. (2011), "Modelling of reinforced concrete structures and composite structures with concrete strength degradation taken into consideration", *Arch. Civil Mech. Eng.*, **11**(3), 623-636.

Kotsovos, M. and Newman, J. (1977), "Behaviour of concrete under multiaxial stress", *Proc. ACI J.*, **74**, 443-446.

Kupfer, H., Hilsdorf, H.K. and Rusch, H. (1969), "Behaviour of concrete under biaxial stresses", *Proc. ACI J.*, **66**, 656-666.

Kupfer, H.B. and Gerstle, K.H. (1973), "Behaviour of concrete under biaxial stresses", *J. Eng. Mech. Div.*, **99**(4), 853-866.

Kwak, H.G. and Filippou, F.C. (1990), "Finite element analysis of reinforced concrete structures under monotonic loads", Department of Civil Engineering, University of California Berkeley, CA.

L´opez-Almansa, F., Alfarah, B. and Oller, S. (2014), "Numerical simulation of RC frame testing with damaged plasticity model. Comparison with simplified models", *Second European Conference on Earthquake Engineering and Seismology*, Istanbul, Turkey,

Lee, S.K., Song, Y.C. and Han, S.H. (2004), "Biaxial behaviour of plain concrete of nuclear containment building", *Nucl. Eng. Des.*, **227**(2), 143-153.

Majewski, S. (2003), *The Mechanics of Structural Concrete in Terms of Elasto-Plasticity*, Silesian Polytechnic Publishing House, Gliwice.

Mills, L.L. and Zimmerman, R.M. (1970), "Compressive strength of plain concrete under multiaxial loading conditions", *J. Am. Concrete Inst.*, **67**(10), 802-807.

Murthy, A.R., Karihaloo, B.L., Iyer, N.R. and Prasad, B.R. (2013), "Determination of size-independent specific fracture energy of concrete mixes by two methods", *Cement Concrete Res.*, **50**, 19-25.

Muthukumar, G. and Kumar, M. (2014), "Failure criteria of concrete-A review", *Comput. Concrete*, **14**(5), 503-526.

Planas, J., Elices, M. and Guinea, G.(1992), "Measurement of the fracture energy using three-point bend tests: Part 2-Influence of bulk energy dissipation", *Mater. Struct.*, **25**(5), 305-312.

RILEM Technical Committee 50-FMC (1985), "Draft recommendation: determination of the fracture energy of mortar and concrete by means of three-point bend tests on notched beams", *Mater. Struct.*, **18**(106), 285-290.

Saenz, L. (1964), "Discussion of equation for the stress-strain curve of concrete, by P. Desayi and S. Krishnan", *ACI J.*, **61**, 1229-1235.

Upreti, G., Murthy, A.R., Goptinath, S., Iyer, N.R. and Venkat, L. (2016), "Strength and ductility of RC beams strengthened with ultra-high strength cementitious composite overlay", *J. Struct. Eng. (Madras)*, **43**(2), 190-198.

Wahalathantri, B.L. (2012), "Damage assessment in reinforced concrete flexural members using modal strain energy based method", Ph.D. Thesis, Queensland University of Technology.

CC